Journal of Power Sources 195 (2010) 1992–1997

Contents lists available at ScienceDirect

Journal of Power Sources

journal homepage: www.elsevier.com/locate/jpowsour

Short communication

Effect of milling intensity on the formation of LiMgN from the dehydrogenation of $LiNH_2$–MgH_2 (1:1) mixture

Jun Lu, Young Joon Choi, Zhigang Zak Fang*, Hong Yong Sohn

Department of Metallurgical Engineering, University of Utah, 135 South 1460 East, Room 412, Salt Lake City, UT 84112, USA

ARTICLE INFO

Article history:
Received 24 September 2009
Received in revised form 12 October 2009
Accepted 13 October 2009
Available online 21 October 2009

Keywords:
Hydrogen storage
LiMgN
Ball milling
Dehydrogenation

ABSTRACT

Metal–N–H systems have recently attracted considerable attention as alternative hydrogen storage materials to traditional metal hydrides. In this work, the reactions of the mixture $LiNH_2$–MgH_2 (1:1) during different mechanical milling processes and the subsequent dehydrogenation reaction were investigated by using TGA, XRD and FT-IR in order to determine an optimal condition for the formation of pure LiMgN. High-energy milling (SPEX mill) and low-energy milling (rolling jar) techniques were used in this work. The results demonstrated that monolithic LiMgN can be produced using the low-energy ball milling technique. The hydrogenation properties of the as-prepared LiMgN were investigated by a Sieverts' type instrument. In contrast, multiple reactions including the metathesis reaction between $LiNH_2$ and MgH_2 and release of H_2 and/or NH_3 took place during high-energy milling using the SPEX mill, which resulted in complicated and unexpected reactions during the subsequent dehydrogenation experiments. Consequently, the dehydrogenated products from the high-energy milled samples consisted of multi-phase mixtures.

1. Introduction

In an effort to develop a reversible hydrogen storage material for vehicular applications, researchers are investigating various metal hydrides/catalysts combinations. Metal–N–H systems [1–21] have recently attracted considerable attention as alternative hydrogen storage materials to the traditional metal hydrides since Chen et al. [1,2] reported reversible hydrogen storage in a mixture of LiH and $LiNH_2$. Among the several reaction systems that were reported in the literature, one particular system that exhibits good reversibility and hydrogen release/uptake properties is the Li–Mg–N–H system [6–21]. Luo and coworkers [6–8] reported that $2LiNH_2$–MgH_2 and $Mg(NH_2)_2$–2LiH could reversibly store more than 5 wt% hydrogen with an equilibrium pressure of around 20 bar at 180 °C [7]. Further investigations indicated that the changes in the molar ratio of $Mg(NH_2)_2$–LiH systems (from 1:1 to 1:4) result in different reaction paths, various amounts of hydrogen released, and different final products [12–18].

More recently, Alapati et al. [22,23] predicted, using first-principle density function theory (DFT) calculations, that the following hydrogen storage system was energetically favorable:

$$LiNH_2 + MgH_2 \rightarrow LiMgN + 2H_2 \quad (1)$$

The above reaction yields 8.2 wt% H_2 and the reaction enthalpy was predicted to be 29.7 kJ mol^{-1} H_2 at 0 K by using the ultra-soft pseudo-potential (USSP) method. Because it is a complete dehydrogenation of both reactants $LiNH_2$ and MgH_2, reaction (1) would be an important reaction for hydrogen storage if it would be reversible and take place at a low temperature. Our earlier experimental findings demonstrated that reaction (1) does take place at temperatures below 260 °C and the dehydrogenated product (LiMgN) can be fully hydrogenated at 160 °C under 2000 psi of H_2 [24]. More detailed theoretical work based on the first-principle calculations of total and vibrational free energies suggests that the reaction between $LiNH_2$ and MgH_2 (1:1) would take place according to the following sequential steps with the final products being LiMgN and H_2 [25]:

$$\begin{aligned} LiNH_2 + MgH_2 &\rightarrow (1/2)Mg(NH_2)_2 + LiH + (1/2)MgH_2 \\ &\rightarrow (1/4)Mg(NH_2)_2 + (1/4)Mg_2N_3 + LiH + H_2 \\ &\rightarrow (1/4)Li_2Mg(NH)_2 + (1/4)Mg_2N_3 + (1/2)LiH + (3/2)H_2 \\ &\rightarrow LiMgN + 2H_2 \end{aligned} \quad (2)$$

Experimentally, Liu et al. [26] showed that the mixture of $LiNH_2$–MgH_2 (1:1) can release 6.1 wt% hydrogen during ball milling and subsequent heating treatments. They also found that the NH_2^- group in $LiNH_2$ and H^- in MgH_2 switched with each other during planetary ball milling, leading to the formation of LiH and $Mg(NH_2)_2$. The newly formed $Mg(NH_2)_2$ then continues to react with the newly formed LiH and/or the remaining MgH_2 to release

* Corresponding author. Tel.: +1 801 581 8128; fax: +1 801 581 4937.
E-mail address: zak.fang@utah.edu (Z.Z. Fang).

0378-7753/$ – see front matter © 2009 Elsevier B.V. All rights reserved.
doi:10.1016/j.jpowsour.2009.10.032

hydrogen at an elevated temperature. The final dehydrogenated products of the study [26] were identified as Mg_2N_3, $Li_2Mg(NH)_2$ and LiH rather than LiMgN [24]. On the other hand, Osborn et al. [27] observed a different product, $Li_2Mg_2(NH)_3$, instead of those from the predicted reaction (1) and (2) after dehydrogenation of the attrition-milled mixture of $LiNH_2$–MgH_2 (1:1) at 210 °C, as expressed in the following reaction:

$$LiNH_2 + MgH_2 \rightarrow (1/3)Li_2Mg_2(NH)_3 + (1/3)MgH_2 + (1/3)LiH + H_2 \quad (3)$$

The above theoretical and experimental findings clearly show that the reactions between $LiNH_2$ and MgH_2 are complex and sensitive to experimental conditions. It appears that parallel reactions may occur during the dehydrogenation process, depending strongly on reaction conditions. Specifically, the sample preparation methods (including ball milling techniques), the usage of catalysts, reaction temperatures, and heating rates may all have important effects on the reaction paths and the final products. For example, the previous studies on this system demonstrated that different ball milling technique resulted in various dehydrogenation kinetics and dehydrogenated products [24,26,27]. It would, therefore, be highly beneficial to investigate how the ball milling techniques affect the dehydrogenation reaction paths of the mixture of $LiNH_2$–MgH_2 (1:1). Understanding the effects of experimental conditions will be critical for determining optimized methods and conditions for the formation of pure LiMgN, which is the key compound in the reversible dehydrogenation/rehydrogenation cycles of this system.

In general, contact or collision between reactant molecules is a necessary condition for a chemical reaction to take place. In the case of solid–solid reactions, such as the reaction studied in the present work, it is especially challenging to bring the reactants together at a molecular level. Ball milling is one of the most effective methods for enabling solid–solid contact. In particular, solid reactants, usually crystalline, may become amorphous which would facilitate reactions during ball milling. During milling, high pressures on the order of GPa are generated on solid particles as the result of high-energy collisions between milling balls, which could initiate not only the primary reactions but also the side reactions. On the other hand, a ball milling process can also be controlled such that the energy of collisions are sufficient for mixing the powders uniformly, but limited to avoid any excessive side reactions that may take place during milling.

The present work investigates the effects of two different types of mechanical ball milling techniques on the reaction between $LiNH_2$ and MgH_2 in 1:1 molar ratio. The two techniques are (a) a low-energy milling technique using a jar-rolling device at low speeds and (b) a high-energy milling technique using a SPEX mill which is a high frequency vibratory mill. An optimal condition for the formation of pure LiMgN from $LiNH_2$ and MgH_2 mixture is proposed based on the results of this study. The results of hydrogenation of the as-prepared LiMgN by using a Sieverts' type instrument (PCTpro-2000) will also be presented.

2. Experimental

The starting materials, lithium amide ($LiNH_2$, 95%), magnesium hydride (MgH_2, 98%) and $TiCl_3$ (98%), were purchased from Sigma–Aldrich Chemical (Milwaukee, WI) and used as received without any further purification. To prevent samples and raw materials from undergoing oxidation and/or hydroxide formation, they were stored and handled in an argon-filled glove box, which maintains low water vapor (less then 1 ppm) and oxygen (less than 1 ppm) concentrations by a recycling purification system. To improve the hydrogenation kinetics, a known catalyst for hydrogen storage reactions, 4 wt% of $TiCl_3$ was added to the material. Ti-based compounds have been found to significantly improve the hydrogen absorption/desorption kinetics for several systems, including $NaAlH_4$ [28], $LiAlH_4$ [29], and $LiNH_2$/LiH [30], although the related mechanism is still not understood well.

Reactant mixtures were prepared using two different ball milling techniques, i.e. the jar-roll mill (low energy; 120 rpm), and SPEX mill (high energy; SPEX SamplePrep 8000-series Mixer/Mills, 1.5 kW h^{-1}) techniques. The same jar with an ID of 3.8 cm and depth of 6.4 cm was used for both mills. Three grams of the mixture of $LiNH_2$ and MgH_2 (1:1) with 4 wt% $TiCl_3$ were loaded into milling jars in the glove box. Stainless steel balls of 0.32 cm in diameter were used. The fraction of jar volume filled with balls and powders was approximately 70%. The milling jar was sealed by a Viton-type o-ring, which enables a constant inert atmosphere during milling. The milling time varied from 0.5 to 4 h in the case of SPEX milling and 12 to 96 h in the case of jar-roll milling.

Thermal gas desorption properties of the milled samples were determined using a thermogravimetric analyzer (TGA) (Shimadzu TGA50) heated to 300 °C using a heating rate of 5° min^{-1}. The TGA instrument was placed inside the argon-filled glove box equipped with a regeneration system, allowing TGA analysis of the material without exposing it to air.

The identification of reactants and reaction products in the mixture before and after the thermogravimetric analysis was carried out using a Siemens D5000 model X-ray diffractometer with Ni-filtered Cu Kα radiation (λ = 1.5406 Å). Each sample for XRD analysis was mounted on a glass slide and covered with a Kapton® tape as a protective film in the glove box. The X-ray intensity was measured over diffraction angle 2θ from 10° to 100° with a scanning rate of 0.02° s^{-1}.

FT-IR spectra were collected using a Bio-Rad spectrometer (FTS-6000) via diffuse reflection of the IR through a loosely packed sample. The FT-IR samples were prepared in an argon-filled glove box by grinding a small amount of the sample with fully dried potassium bromide (KBr) powder in an agate mortar and pestle. The ground sample was then transferred and loosely packed into a custom holder, which is approximately 7 mm in diameter and 3 mm in thickness. The sample holder was then removed from the glove box and immediately transferred to a spectrometer. The samples were placed one at a time into the sample compartment of the spectrometer. After mounting a sample in place the sample compartment was purged by nitrogen for approximately 25 min prior to collection of the spectrum. Each spectrum shown in this paper used the spectrum from the blank KBr powder for the background.

The hydrogenation of dehydrogenated samples was evaluated by using a commercial Sieverts' type apparatus (PCTPro-2000). About 1.5 g of sample was loaded into a stainless steel container, which was then sealed in the PCT autoclave in the glove box. Hydrogen pressures were measured by a Teledyne Taber model 206 piezoelectric transducer, 0–20 MPa, with a resolution of 10^{-4} MPa. During dehydrogenation/hydrogenation, the sample temperature and applied pressure were monitored and recorded by a Lab View-based software program. The amount of hydrogen release/uptake was calculated based on the pressure changes in calibrated volumes. The details of PCT measurement are described elsewhere [31].

3. Results and discussion

3.1. Reaction between $LiNH_2$ and MgH_2 during ball milling and subsequent dehydrogenation process

In order to determine the optimized condition for the formation of monolithic LiMgN from the mixture of $LiNH_2$–MgH_2 (1:1), two

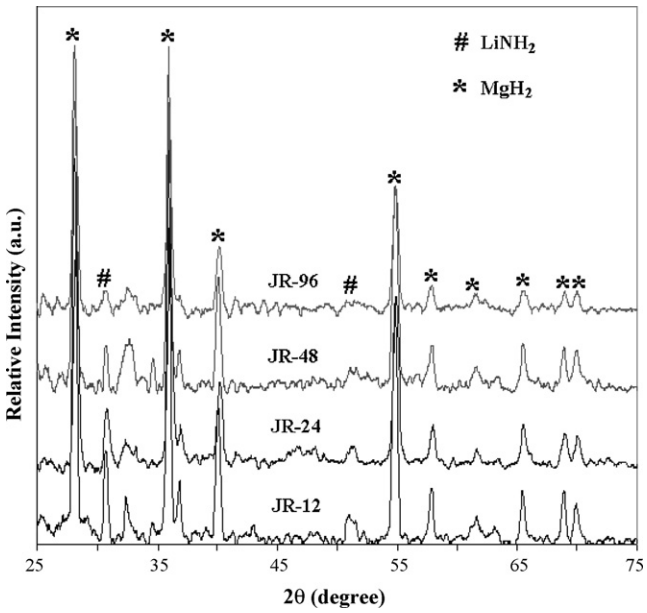

Fig. 1. XRD patterns of the $LiNH_2$–MgH_2–4 wt%$TiCl_3$ mixtures after jar-roll milling for different lengths of time.

different mechanical ball milling methods were used, as described earlier. For the purpose of discussion, the milled samples are designated as JR-H or SP-H, where JR represents the jar-roll milling method, SP represents the SPEX milling method, and H indicates the length of time of milling in hours.

3.1.1. Low-energy ball milling (jar-roll milling)

To investigate possible reactions during the milling processes, X-ray diffraction analysis (XRD) were carried out on the samples after ball milling. Fig. 1 shows a series of XRD patterns of the JR-H samples. It shows that both $LiNH_2$ and MgH_2 phases are preserved after jar-roll milling. Because XRD patterns of $LiNH_2$ and Li_2NH are very similar, FT-IR analysis is also conducted to verify the presence of $LiNH_2$ or Li_2NH in milled samples. Fig. 2 shows the FT-IR spectra of JR-H samples. The typical peaks representing doublet N–H asymmetric and symmetric vibrations of the amide group in $LiNH_2$ at 3313 and 3259 cm^{-1} are present for all JR-H samples. In other words, the predicted thermodynamically stable phases of $Mg(NH_2)_2$ and LiH [25] were not observed, indicting no reactions took place during the low-energy jar-roll milling.

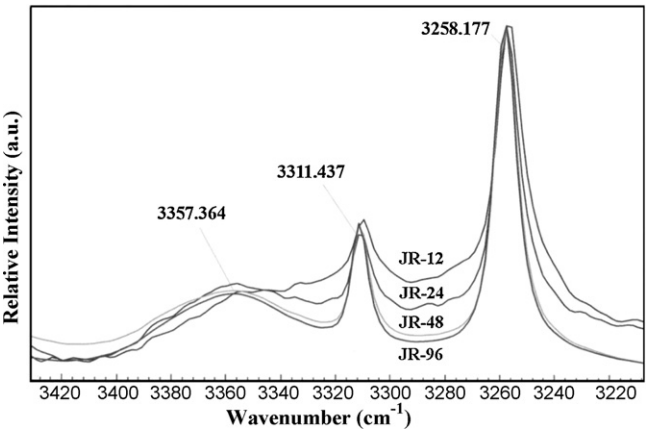

Fig. 2. FT-IR spectra of the $LiNH_2$–MgH_2–4 wt%$TiCl_3$ mixtures after jar-roll milling for different lengths of time.

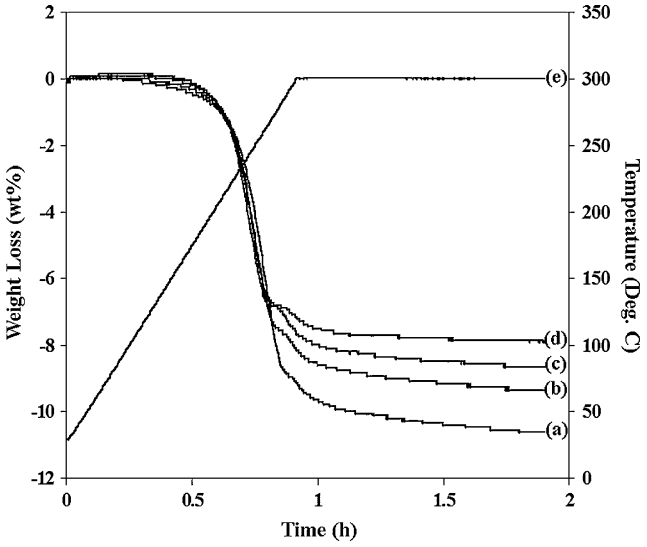

Fig. 3. TGA profiles of the $LiNH_2$–MgH_2–4 wt%$TiCl_3$ mixtures after jar-roll milling for different lengths of time: (a) 12 h, (b) 24 h, (c) 48 h, (d) 96 h, and (e) the temperature profile.

Although $LiNH_2$ and MgH_2 did not react during low-energy milling, the XRD diffraction peaks broadened during the ball milling process, suggesting that the low-energy ball milling effectively reduced the grain size of the raw materials. Overall, the low-energy milling uniformly mixed the raw materials without causing any chemical reactions, which allowed us to investigate the reactions in subsequent controlled dehydrogenation experiments using TGA.

Fig. 3 shows the weight loss versus temperature curves of the same series of JR-H samples measured using TGA. The experiments were run under argon atmosphere with a heating rate of 5 °C min^{-1}. The weight loss of the samples that were milled for less than 48 h was higher than the theoretical hydrogen capacities (8.2 wt%) according to reaction (1). This difference was attributed to the formation of NH_3 gas released during the dehydrogenation process, which could occur if the powders were not uniformly mixed. When the time of milling was increased to 96 h, the weight loss of the samples during TGA analysis were approximately equal to the theoretical hydrogen capacity of the material, suggesting that the dehydrogenation reaction was completed without significant release of NH_3 gas. These results demonstrate that milling time is a critical factor affecting the uniformity of the mixture, thus the reactions during dehydrogenation.

Fig. 4 shows the XRD patterns of the dehydrogenated JR-12 and JR-96 samples. To identify possible phases contained in the dehydrogenated samples, the XRD patterns for selected pure materials, which may be parts of the dehydrogenated products, are also shown in Fig. 4 as vertical bars for comparison. It clearly shows that LiMgN was the primary phase in the dehydrogenated JR-96 sample, while a mixture of LiMgN and Mg_3N_2 was observed in the dehydrogenated JR-12 sample. From the above results, it can be inferred that when a low-energy milling technique such as the jar-rolling technique is used, milling time must be sufficiently long to ensure that uniform mixing of $LiNH_2$ and MgH_2 is achieved, which is necessary for the formation pure LiMgN from the subsequent dehydrogenation process.

3.1.2. High-energy ball milling (SPEX Mill milling)

The results are more complicated when a high-energy ball milling technique (SPEX mill) is used. Fig. 5 shows the TGA profiles of a series of SP-H samples. First, the samples that were SPEX milled for 0.25 and 0.5 h (SP-0.25 and SP-0.5) showed 10.4 and 9.6 wt% of weight loss, respectively, which are higher than the theoretical

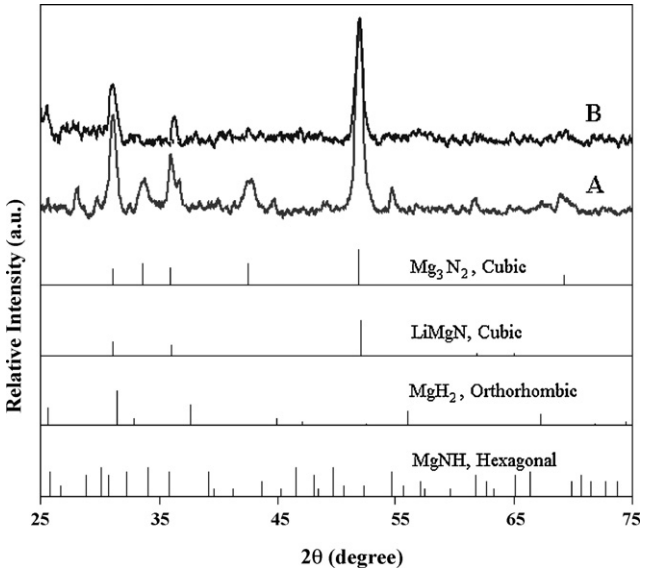

Fig. 4. XRD patterns of the $LiNH_2$–MgH_2–4 wt%$TiCl_3$ mixtures after jar-roll milling for different lengths of time and then dehydrogenated at 300 °C: (a) dehydrogenated JR-12 sample and (b) dehydrogenated JR-96 sample.

hydrogen capacity (8.2 wt% based on reaction (1)) of the mixture, suggesting that NH_3 gas was released during the dehydrogenation process. This can be explained by the fact that the mixtures were milled for only a very short time, hence could not have been uniformly mixed. When the ball milling time increased to 1 h, the weight loss of the sample SP-1 measured by TGA was 7.9 wt%, suggesting that the dehydrogenation process was complete (theoretical capacity is 8.1) without significant release of NH_3. However, as the SPEX milling time was further increased, the weight losses of the samples SP-2 and SP-4 were only 5.4 and 3.8 wt%, respectively, drastically lower than the theoretical hydrogen capacity. This strongly indicates that complex reactions occurred during the high-energy SPEX milling when the milling time is increased to longer than 2 h.

To understand the chemical reactions that occurred during the high-energy ball milling process, solid residues at different milling stages were collected for XRD and FT-IR analysis. Fig. 6 shows the

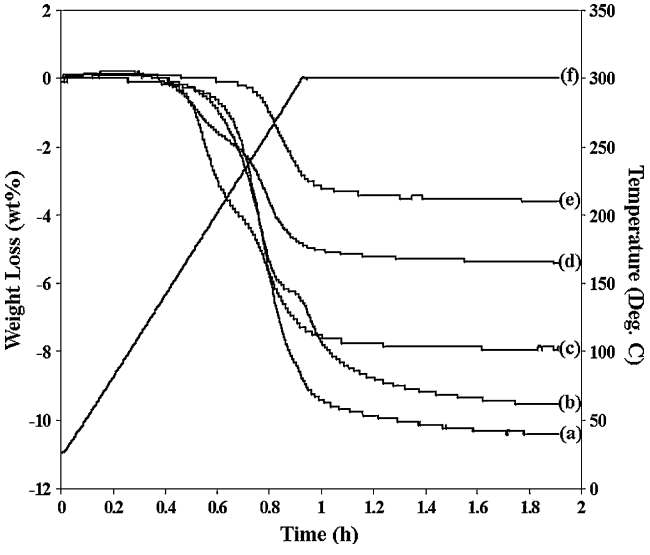

Fig. 5. TGA profiles of the $LiNH_2$–MgH_2–4 wt%$TiCl_3$ mixtures after SPEX milling for different lengths of time: (a) 0.25 h, (b) 0.5 h, (c) 1 h, (d) 2 h, (e) 4 h, and (f) the temperature profile.

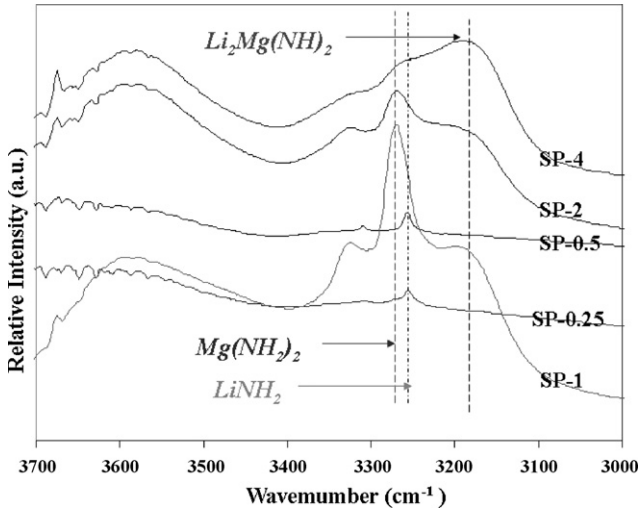

Fig. 6. FT-IR spectra of the $LiNH_2$–MgH_2–4 wt%$TiCl_3$ mixtures after SPEX milling for different lengths of time.

FT-IR spectra of a series of SP-H samples. The samples SP-0.25 and SP-0.5 exhibit the typical doublet N–H asymmetric and symmetric vibrations of the amide group in $LiNH_2$ at 3313 and 3259 cm^{-1}, respectively, indicating that no reactions took place during the short duration of the high-energy ball milling process.

However, the characteristic N–H vibrations of $LiNH_2$ became almost invisible when the milling time is increased to 1 h. The new doublets at 3274 and 3325 cm^{-1} are the characteristic N–H asymmetric and symmetric vibrations of the amide ions in $Mg(NH_2)_2$. In addition to the two absorption peaks of $Mg(NH_2)_2$, there is another new absorbance peak at 3190 cm^{-1} at the same time, which is in the N–H vibration range of imides. This peak can be assigned to the N–H vibration in $Li_2Mg(NH)_2$ or MgNH as proposed in the literature [28].

The above results indicates that high-energy ball milling induces the exchange of the NH_2^- group and H^- between $LiNH_2$ and MgH_2 and the formation of $Mg(NH_2)_2$, as expressed in the following reaction:

$$LiNH_2 + MgH_2 \rightarrow (1/2)Mg(NH_2)_2 + LiH + (1/2)MgH_2 \quad (4)$$

Subsequently, the newly formed $Mg(NH_2)_2$ may react with the newly formed LiH or the residue MgH_2 in the starting material according to the following equations:

$$(1/2)Mg(NH_2)_2 + LiH \rightarrow (1/2)Li_2Mg(NH)_2 + H_2 \quad (5)$$

$$Mg(NH_2)_2 + MgH_2 \rightarrow 2MgNH + 2H_2 \quad (6)$$

As can be seen, reactions (5) and (6) produce H_2 and $Li_2Mg(NH)_2$ or MgNH. It should be emphasized that reactions (4)–(6) occurred all under the high-energy ball milling conditions (SPEX mill). When the SPEX milling time was further prolonged to 4 h, the characteristic peaks of N–H vibrations in $Mg(NH_2)_2$ gradually disappeared and the absorbance peak at 3190 cm^{-1} became broader and stronger, suggesting that reactions (5) and/or (6) continued until $Mg(NH_2)_2$ formed by reaction (4) was consumed.

Fig. 7 illustrates the XRD patterns of the same series of SP-H samples. It can be seen that the samples milled for the first 0.5 h (SP-0.25 and SP-0.5) consisted of only the original $LiNH_2$ and MgH_2 phases, which is in agreement with the FT-IR analysis. This result shows that reaction (4) did not take place in the early stage of high-energy ball milling, which is similar to the results of the low-energy ball milling (jar-roll mill) experiments. After 1 h of SPEX milling, the diffraction peaks of $LiNH_2$ became invisible although the MgH_2 phase was still clearly present in the XRD pattern. Two small peaks

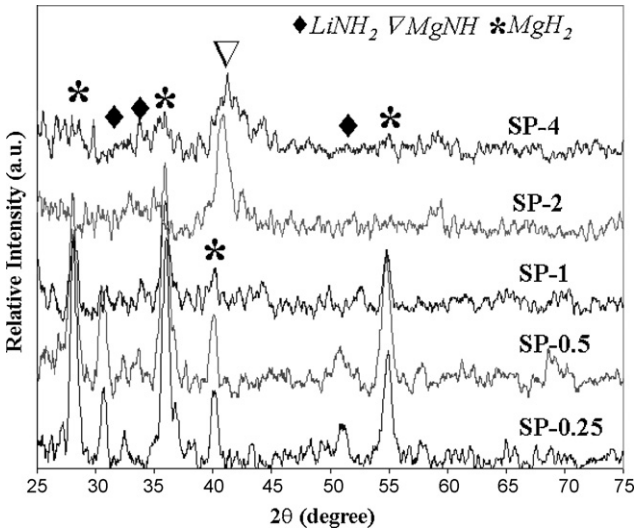

Fig. 7. XRD patterns of the $LiNH_2$–MgH_2–4 wt%$TiCl_3$ mixtures after SPEX milling for different lengths of time.

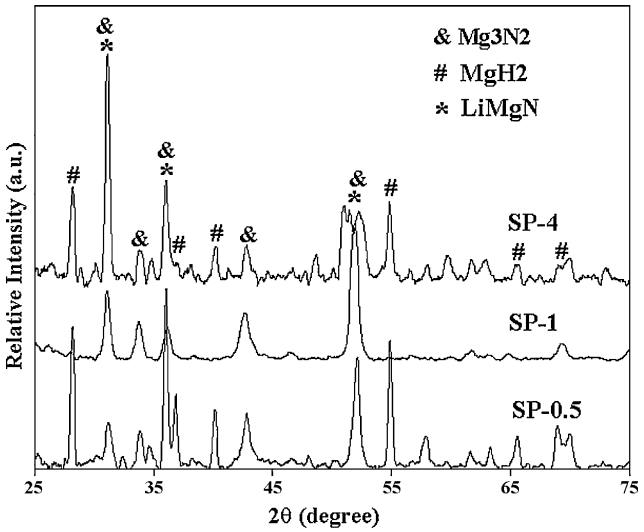

Fig. 8. XRD patterns of the $LiNH_2$–MgH_2–4 wt%$TiCl_3$ mixtures after SPEX milling for different lengths of time and then dehydrogenated at 300 °C: (a) dehydrogenated SP-0.5 sample, (b) dehydrogenated SP-1 sample, and (c) dehydrogenated SP-4 sample.

were observed at 38° and 44° (2θ), which can be assigned to LiH phase, using the JCPDS-ICDD database. This result indicates that there was a chemical reaction between $LiNH_2$ and MgH_2 during the high-energy ball milling, which should be reaction (4) according to Refs. [25,26]. However, the diffraction peaks of $Mg(NH_2)_2$, one of the expected products according to reaction (4), were not visible in the XRD pattern. This was possible if the $Mg(NH_2)_2$ phase was amorphous as a result of the high-energy milling. When the milling time was further increased to 2–4 h, the diffraction peaks of MgH_2 also disappeared completely, indicating that MgH_2 was either consumed by a reaction with the newly formed $Mg(NH_2)_2$ or became amorphous due to the high-energy milling. Another broad peak was observed at 41.5° in the XRD patterns of samples SP-2 and SP-4, which can be assigned to MgNH phase based on literature studies [32].

On the basis of the above results and discussions, the reactions and changes during high-energy ball milling (SPEX mill) of the $LiNH_2$–MgH_2 mixture can be qualitatively understood as follows: first, no reaction occurs during the initial stage of milling (<0.5 h). The exchange of NH_2^- group and H^- between $LiNH_2$ and MgH_2 based on reaction (4) takes place when the milling time increases to longer than 1 h. When the milling time further increase to longer than 2 h, one of the products of reaction (4), $Mg(NH_2)_2$, reacts with MgH_2 and/or LiH to form corresponding imides while releasing H_2 according to reactions (5) and (6).

Due to the multi-step reactions during the high-energy ball milling and subsequent dehydrogenation process, the dehydrogenated samples are expected to be mixtures of various phases. Fig. 8 shows the XRD profiles of the dehydrogenated SP-H samples. Apparently, all the dehydrogenated SP-H samples show multi-phase compositions comprised of cubic LiMgN, cubic Mg_3N_2, unreacted MgH_2, and minor amounts of imide phases. These results strongly support the hypothesis that the reactions and products of $LiNH_2 + MgH_2$ during dehydrogenation at a moderate temperature (200–300 °C) depend on the method of preparation of the mixture of the reactants. A high-energy ball milling technique will likely lead to multi-step reactions and mixtures of multiple phases as the products, while a suitable low-energy milling technique does not cause any reactions and produces monolithic LiMgN. It should be pointed out that more detailed studies are still needed to pinpoint the reaction mechanisms as functions of experimental conditions. For example, it was also found in this study that the temperature and heating rate during the dehydrogenation process also have critical effects on the compositions of the final products, which are the subjects of on-going investigations by the present authors.

3.2. Hydrogenation of LiMgN

An isothermal hydrogenation experiment using a PCT apparatus was performed on the dehydrogenated sample JR-96 to verify the ability of LiMgN for hydrogenation, as shown in Fig. 9. The hydrogenation experiment was carried out under a hydrogen pressure of 160 bar at 180 °C. It can be seen that a total of 8.0 wt% hydrogen was picked up by the as-prepared LiMgN, illustrating that under the present testing condition the dehydrogenated $LiNH_2 + MgH_2$ sample can be completely reversed in terms of its hydrogen content. The XRD pattern and FT-IR spectrum of the rehydrogenated sample, however, showed no $LiNH_2$ phase, suggesting that the hydrogenation reaction did not follow that of the reverse reaction of Eq. (1). The results of hydrogenation experiments showed that that the rehydrogenation process of LiMgN depends strongly on the hydrogen pressure and hydrogenation temperature under the conditions used in the current studies. Details of the study on the

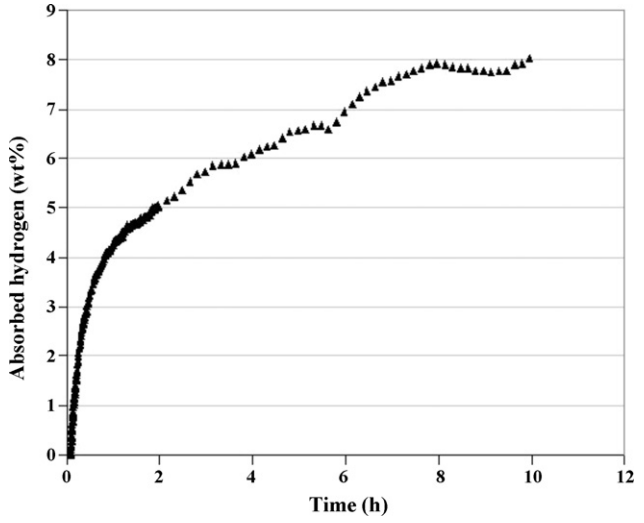

Fig. 9. Isothermal H_2 absorption curve of the $TiCl_3$-doped LiMgN (dehydrogenated JR-96 sample) under 160 bar at 180 °C.

hydrogenation reactions of LiMgN will be reported in a separate paper.

4. Conclusions

It is concluded based on the results of this study that ball milling technique and conditions have critical effects on the dehydrogenation products from a mixture of $LiNH_2$–MgH_2. An optimal condition for the formation of pure LiMgN is to use low-energy ball milling technique to mill the raw materials ($LiNH_2$ and MgH_2) for a sufficiently long time (96 h or more in the current study) to uniformly mix the material and create intimate contact between the reactants, without triggering reactions during the milling process. Monolithic LiMgN can then be obtained by heating the milled $LiNH_2$–MgH_2 mixture to 200–300 °C under argon. If a high-energy ball milling technique is used for mixing and milling of the raw materials, multiple steps of reactions between $LiNH_2$ and MgH_2 are expected to take place during milling, which further complicates the reactions during subsequent heating, resulting in multi-phase mixtures as the product. In short, direct milling of $LiNH_2$–MgH_2 using a high-energy milling technique such as SPEX mill is not suitable for preparing pure LiMgN. The as-prepared LiMgN using the low-energy ball milling method can be fully rehydrogenated.

Acknowledgments

The authors wish to thank Dr. Jan Miller and Dr. X. Wang for their assistance with FT-IR analysis. This research was supported by the U.S. Department of Energy (DOE) under contract number DE-FC36-05GO15069.

References

[1] P. Chen, Z. Xiong, J. Luo, J. Lin, K.L. Tan, Nature 420 (2002) 302.
[2] P. Chen, Z. Xiong, J. Luo, J. Lin, K.L. Tan, J. Phys. Chem. B 107 (2003) 10967.
[3] J. Lu, Z.Z. Fang, J. Phys. Chem. B 109 (2005) 20830.
[4] J. Lu, Z.Z. Fang, H.Y. Sohn, J. Phys. Chem. B 110 (2006) 14236.
[5] J. Lu, Z.Z. Fang, H.Y. Sohn, Inorg. Chem. 45 (2006) 8749.
[6] W. Luo, J. Alloys Compd. 381 (2004) 284.
[7] W. Luo, E. Ronnebro, J. Alloys Compd. 404–406 (2005) 392.
[8] W. Luo, Q. Sickafoose, J. Alloys Compd. 407 (2006) 274.
[9] Z. Xiong, G. Wu, J. Hu, P. Chen, Adv. Mater. 16 (2004) 1522.
[10] Z. Xiong, J. Hu, G. Wu, P. Chen, W. Luo, K. Gross, J. Wang, J. Alloys Compd. 398 (2005) 235.
[11] Z. Xiong, J. Hu, G. Wu, P. Chen, W. Luo, J. Wang, J. Alloys Compd. 417 (2006) 190.
[12] H.Y. Leng, T. Ichikawa, S. Hino, N. Hanada, S. Isobe, H. Fujii, J. Phys. Chem. B 108 (2004) 8763.
[13] H.Y. Leng, T. Ichikawa, S. Hino, T. Nakagawa, H. Fujii, J. Phys. Chem. B 109 (2005) 10744.
[14] H.Y. Leng, T. Ichikawa, H. Fujii, J. Phys. Chem. B 110 (2006) 12964.
[15] Y. Nakamori, G. Kitahara, K. Miwa, N. Ohba, T. Noritake, S. Towata, S. Orimo, J. Alloys Compd. 404–406 (2005) 396.
[16] T. Ichikawa, K. Tokoyoda, H.Y. Leng, H. Fujii, J. Alloys Compd. 400 (2005) 245.
[17] M. Aoki, T. Noritake, G. Kitahara, Y. Nakamori, S. Towata, S. Orimo, J. Alloys Compd. 428 (2007) 307.
[18] Y. Nakamori, G. Kitahara, K. Miwa, S. Towata, S. Orimo, Appl. Phys. A 80 (2005) 1.
[19] J. Rijssenbeek, Y. Gao, J. Hanson, Q. Huang, C. Jones, B. Toby, J. Alloys Compd. 454 (2008) 233.
[20] J. Yang, A. Sudik, C. Wolverton, J. Alloys Compd. 430 (2007) 334.
[21] Y. Liu, K. Zhong, K. Luo, M. Gao, H. Pan, Q. Wang, J. Am. Chem. Soc. 131 (2009) 1862.
[22] S.V. Alapati, K.J. Johnson, D.S. Sholl, J. Phys. Chem. B 110 (2006) 8769.
[23] S.V. Alapati, K.J. Johnson, D.S. Sholl, Phys. Chem. Chem. Phys. 9 (2007) 1438.
[24] J. Lu, Z.Z. Fang, Y.J. Choi, H.Y. Sohn, J. Phys. Chem. C 111 (2007) 12129.
[25] A.R. Akbarzadeh, V. Ozolins, C. Wolverton, Adv. Mater. 19 (2007) 3233.
[26] Y. Liu, K. Zhong, M. Gao, J. Wang, H. Pan, Q. Wang, Chem. Mater. 20 (2008) 3521.
[27] W. Osborn, T. Markmaitree, L.L. Shaw, J. Power Sources 172 (2007) 376.
[28] B. Bogdanovic, M. Schwickardi, J. Alloys Compd. 253 (1997) 1.
[29] J. Chen, N. Kuriyama, Q. Xu, H.T. Takeshita, T. Sakai, J. Phys. Chem. B 105 (2001) 11214.
[30] S. Isobe, T. Ichikawa, N. Hanada, H.Y. Leng, M. Fichtner, O. Fuhr, H. Fujii, J. Alloys Compd. 404–406 (2005) 439.
[31] W. Luo, J.D. Clewley, T.B. Flanagam, J. Less-Common Metals 141 (1988) 103.
[32] J. Hu, G. Wu, Y. Liu, Z. Xiong, P. Chen, K. Murata, K. Sakata, G. Wolf, J. Phys. Chem. B 110 (2006) 14688.